SEMARAK ILMU PUBLISHING

Journal of Advanced Research in Applied Sciences and Engineering Technology

Journal homepage:
https://semarakilmu.com.my/journals/index.php/applied_sciences_eng_tech/index
ISSN: 2462-1943

MRI T1-Weighted Fat Segmentation Based on Active Contour for Osteosarcoma Patients

Muhammad Shauqi Muhammad Shukor[1], Belinda Chong Chiew Meng[1,*], Nor Salwa Damanhuri[1], Nor Azlan Othman[1], Mohamad Haizan Othman[1,2], Mohd Ezane Aziz[2]

[1] Biomedical Engineering and Intelligent System (BioMIS) Research Group, Centre for Electrical Engineering Studies, Universiti Teknologi MARA, Cawangan Pulau Pinang, 13500 Permatang Pauh, Pulau Pinang, Malaysia
[2] Department of Radiology, Universiti Sains Malaysia, Jalan Raja Perempuan Zainab II, Kubang Kerian, 16150 Kota Bharu, Kelantan, Malaysia

ARTICLE INFO

Article history:
Received 5 November 2023
Received in revised form 9 May 2024
Accepted 30 May 2024
Available online 31 July 2024

Keywords:
Active contour; fat segmentation; MRI; multilevel thresholding; osteosarcoma; T1-Weighted

ABSTRACT

Osteosarcoma (OS) is the most common and frequent primary bone cancer in children and adolescents. This type of bone cancer often developed at the long bones' extremities close to the metaphyseal growth plates. To address these issues, OS quantitative analysis is performed using Magnetic Resonance Imaging (MRI) to plan surgical procedures and track the effectiveness of treatment. Fat suppression is commonly employed to eliminate the fat signal from T1-Weighted MRI sequence. The suppressed fat signal in T1-Weighted is important and often used to identify abnormalities in other MRI sequences. In clinical, MRI images must be interpreted by a radiologist. Manually outlining the tumour location is laborious and subjective. Image processing involves segmentation to separate information from the desired target region of the image. Active Contour (AC) is an algorithm often used in medical images for segmentation. Nevertheless, the process of mask initialization can be challenging and requires careful attention. This study proposes a method to define the mask initialization so that the AC has a starting point to extract fat in T1-Weighted for the purpose of fat suppression. From the results obtained, AC with the proposed mask initialization method successfully segmented the fat in T1-Weighted MRI images with accuracy, precision, recall and F1-score of 0.92, 0.86, 0.88 and 0.89 respectively.

1. Introduction

1.1 Research Background

OS is a primary malignant tumour of the skeleton that mostly affects the long bones where osteoid or immature bone tissue is formed by sarcoma cells [2]. The anatomical location of the lesion is frequently a factor in the diagnosis of bone tumours [3]. OS is no exception, with the metaphysis of the femur, tibia, or humerus being the typical site of traditional OS.

Currently, OS quantitative analysis is carried out using non-invasive methods to schedule operations and monitor the efficacy of treatment. Magnetic Resonance Imaging (MRI) image is one

* *Corresponding author.*
E-mail address: belinda.chong@uitm.edu.my

https://doi.org/10.37934/araset.49.2.114

of the common imaging methods that are often used in the medical field for clinical analysis [4]. MRI is crucial for figuring out the tumour's location within the bone and the size of any associated soft tissue mass.

There are a few types of MRI image sequences that are often used in medical diagnosis, for example T1-Weighted, T2-Weighted and STIR sequence. T1-Weighted images are good in exhibiting fat tissue as the highest signal, suited to displaying anatomical structures. T2-Weighted imaging gives the highest signal in fluids which are the best indicator for lesions. While STIR sequence is the best in describing lesions that contain abnormal fluid in the MRI image [5].

Fat suppression method is crucial for musculoskeletal imaging. This method eliminates the fat contribution from T1-Weighted with no impact on the water signal. The method used to distinguish high-signal-intensity structures on T1-Weighted which rule out the presence of fat in soft-tissue tumours and improve presentation of bone-marrow edema or lesions in T2-Weighted images [6].

Radiologists are specialized medical doctors who primarily utilize medical imaging techniques. The interpretation of MRI images can be very subjective, influenced by the level of experience of radiologists. Differentiation between fat and muscle can vary among radiologists based on their individual experiences in the medical field [6]. Manually defining the location of OS is a tedious and draining procedure especially when radiologists must evaluate each one of MRI image sequences for only a patient. More difficulties come from numerous pixel textures within the tumour itself and the tumorous tissues' uncanny resemblance to neighbouring healthy tissues [5].

Developing an automatic segmentation system for separating muscles and fats in T1-Weighted axial images of the long bone is a crucial step in medical imaging analysis. Accurate and efficient segmentation of muscles and fats can provide valuable information for various applications, such as monitoring muscle changes due to age, disease, or treatment, assessing body composition, and aiding in surgical planning [7].

Image segmentation is a technique to separate the original image into various parts and extracts the useful sections based on the many image characteristics [8]. Active Contour (AC) is a type of segmentation technique that uses energy forces and limitations to separate the pixels of interest from a picture for further processing and analysis [9]. AC is referred to as an active segmentation model. A contour is an array of points that have been interpolated. The interpolation process might be linear, spline-based, or polynomial, depending on the image's curve. AC are mostly used in image processing to define smooth shapes in images and create closed contours for certain regions [10]. In this context, AC algorithm is used in the medical field to separate fat and muscles in MRI images [11]. AC is good for segmentation when the mask placed on the long bone must include both fat and muscle regions with an appropriate number of iterations. However, the seed initialization often can be very difficult [12].

1.2 Literature Review

AC, also known as snake model, is a type of image processing algorithm that locates edges by using boundaries. This segmentation algorithm uses energy forces and limits to separate the pixels of interest from an image for further processing and analysis [13]. The edges are detected by moving the boundaries along the images and it will stop the mask movement at the edges of the object. This method is commonly used to trace objects, particularly in medicine.

Mustafa *et al.,* [14] developed an automated system for detecting skin cancers through image processing, addressing issues such as image noise (e.g., shadows, hairs), low contrast, and specular reflection that can hinder accurate lesion detection. The AC algorithm was employed to identify abnormal skin lesions. Comparatively, the results obtained from the Gaussian filter-based maximum

entropy-based threshold and adaptive contour algorithm showed improvements over the image segmentations performed by expert dermatologists [14].

Huo *et al*., [15] conducted a research study focusing on the efficacy evaluation of ultrasound with an active contour model for haemodialysis in children with renal failure [15]. The aim of this study was to support haemodialysis procedures in paediatric patients with renal failure by investigating the effectiveness of the ultrasound combined with an AC model. The study employed a pulse coupled neural network (PCNN) to extract the initial shape of ultrasound images, followed by accurate segmentation using an AC model based on a cloud model. The error rate of the AC algorithm model was 11.01%, much lower than the error rate of the classical Snake model, which had a rate of 18.87% ($P<0.05$) [15].

Mewada *et al.,* [16] proposed a semi-automatic model for addressing challenges related to significant variability in image modalities and limitations in instrument acquisition processes, with a focus on segmenting medical images. The results of the comparative analysis demonstrated the robustness of the proposed model against noise and its ability to successfully segment medical images from different modalities, achieving an average accuracy of 99.57% [16].

Another research which involves the use of AC is by Babu *et al*., [17]. In the study they highlight that manual assessment of an MRI images are too tedious and vexing for the doctors, therefore they conclude that the usage of computerise analysis is crucial. In the study, they determined the effective way to detect the brain tumour from the MRI images using AC segmentation technique. The study consists of the processes of inserting the image, processed the image to enhance the quality and removing any part which may disturb the segmentation such as the skull, threshold and segmenting using Chan-Vese (C-V) method and Level Set method (LSM).

Ibrahim *et al.,* proposed a new deformable AC based model using on fractional Wright function for tumour segmentation of volumetric MRI brain scans [18]. The proposed method generalised boundary tracking in AC segmentation by using fractional calculus as a minimization energy function to replace the usual gradient-descent method. The performance of the proposed method was tested using dice similarity index. The proposed method can perform better than the standard active contour with sensitivity score of 94.8%.

Thresholding is the simplest technique for segmenting images in digital image processing. Otsu's is one of the common techniques used for image thresholding to convert grayscale images to binary images [19]. Otsu's thresholding aims to automatically determine an optimal threshold value to separate an image into foreground and background regions based on the image's histogram. In Otsu's approach, the threshold between background and foreground is examined for every conceivable value. Otsu's technique works effectively when the histogram has a bimodal distribution with a deep and acute valley between the two peaks. However, Otsu's technique is ineffective if there is the presence of noise, or greater intra-class than inter-class variance [20].

Multilevel thresholding divides an image with grey levels into a few separate sections. This method selects multiple thresholds for the target image and divides it into distinct brightness regions, each of which corresponds to a different background and different objects [21]. Su *et al*., [22] proposed a method based on multilevel thresholding image segmentation (MTIS) to improve the processing efficiency of COVID-19 chest films. They introduce horizontal and vertical search mechanisms from the original multi-verse optimizer to obtain higher quality segmentation results. The study provides an efficient segmentation technique to process COVID-19 chest radiography and subsequently assist medical professionals in diagnosing coronavirus pneumonia.

Otsu's multi-level thresholding is an extension of Otsu's thresholding, which is a widely used method for image thresholding. There are some research works that use Otsu multi-level thresholding for image processing. Song *et al.,* [23] explores the application of Otsu's multilevel

Threshold Algorithm. The researchers emphasized an enhanced approach to adjust the threshold bias in Otsu's algorithm, taking into consideration the observation that the algorithm tends to set the threshold closer to the class with the largest intraclass variation in cases where there are significant differences in intraclass variances between the foreground and background. The proposed method exhibited significantly reduced time consumption.

The utilization of Otsu's multilevel threshold algorithm is also highlighted in a study conducted by Al-Rahlawee and Rahebi [24]. Even though they obtain high accuracy and efficiency in the study, these methods exhibit high computational complexity. This is because, as the number of thresholds used increases, their efficiency is compromised due to the associated increase in complexity and execution time [24].

Based on the review, it shows that multilevel thresholding could divide an image into several regions based on its histogram distribution. The method performs well for multi-modal histogram thresholding. On the other hand, AC algorithm has been widely used in medical image processing. The integration of multilevel thresholding and AC can produce a smooth and accurate segmentation; thus, it is the best method used to extract fat. However, the drawback of AC algorithm is its need initial contour as input parameters to begin the process of segmentation. The mask initialization placement is important, the accuracy of the algorithms hugely depends on the size and placement of the mask. Therefore, more study should be ventured on mask initialization for search process in the beginning process. The goal of this study is to propose a method to define an initialization mask so that the AC algorithm has an initial point to start the search process. With the initialization mask, the AC algorithm starts to contract or expand in the process of fat extraction. The fat extracted from T1-Weighted can be used to eliminate the fat signal in other MRI sequences so that the visibility of abnormality can be improved.

2. Methodology

This study proposes a method for defining a mask initialization so that the AC algorithm has a starting point from which to begin its search phase. The methodology of this study consists of four main parts which are data acquisition, image pre-processing, define AC mask initialization for fat extraction and performance evaluation. Figure 1 shows the block diagram of the study.

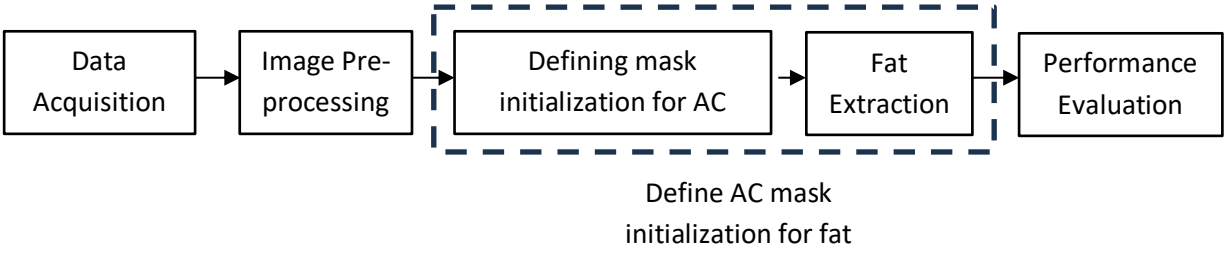

Fig. 1. Block diagram of the project

2.1 Data Acquisition

All 43 data collected were patients that were diagnosed with Osteosarcoma in the long bone (femur and tibia). MRI T1-Weighted images were collected from Hospital Universiti Sains Malaysia. This study has obtained an ethical approval from Jawatankuasa Etika Penyelidikan Manusia (JEPeM) with ethic number of USM/JEPeM/22060378. The T1-Weighted image modality is employed to highlight fat tissue, showcasing it as the highest signal. Generally, the fat layer in T1 images is depicted

with higher intensity. In this study, only the axial plane is used. Axial plane is the basic plane of an MRI image where the image is slice from bottom to top of human body.

2.2 Image Pre-Processing

Image pre-processing is a process to remove extraneous background noise. This process is important as the AC algorithm requires the application of region of interest (ROI) mask for image segmentation. To achieve improved segmentation results, the T1-Weighted image input undergoes cropping to enhance the process. This is to increase accuracy and reduce the complexity of segmentation in the next process.

In this study, the ROI is the bone which is covered by fat and muscle. The outer region is fat that first needs to be extracted. Figure 2(a) shows the original T1-Weighted image from one of the data acquisitions. Figure 2(b) is the histogram of the T1-Weighted image. In the histogram there are three distinct regions observed which are background, muscle, and fat. Multi-level thresholding is used to segment a grayscale image into different regions. The process begins by binarizing the original image, segmenting the fat region as foreground and other as background into two distinct gradients (1 and 0). Next, the objects that are connected to the border are then removed.

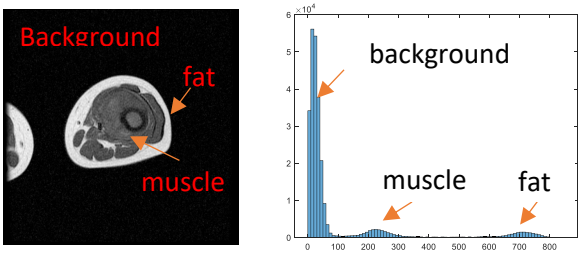

Fig. 2. (a) Original T1-Weighted image (b) Histogram of T1-Weighted

One of challenges in this process is inhomogeneity. Inhomogeneity refers to the presence of variations or irregularities in the intensity. Inhomogeneity happens because of edema or inflammation that contains abnormal fluids in the muscle which form irregular anatomical area to occur in the T1-Weighted MRI image. Because fluids cannot be displayed in T1-Weighted images; therefore, the fat cannot be fully covered in the images that have inhomogeneity. Morphological dilation is applied to cover the irregular fat region due to the inhomogeneity. The image is then filled and dilate till the image obtains the largest area to eliminate the inhomogeneity effect. Next, the bounding box of the ROI is defined. The background pixel is then assigned with zero to eliminate the background noise.

2.3 Defining AC Mask Initialization for Fat Extraction

AC is a segmentation technique that uses local energy force and limitation to separate objects. Contours are lines defining the area of interest in an image and are made up from a set of interpolated points. Eq. (1) is used to define the sum of the snake's internal and external energy.

$$E^*_{snake} = \int_0^1 E_{snake}\big(V(s)\big)ds == \int_0^1 \Big(E_{internal}\big(V(s)\big) + E_{image}\big(V(s)\big) + E_{con}\big(V(s)\big)\Big)\,ds \qquad (1)$$

Where $E*_{snake}$ is a simple elastic snake that defined by a set of n points V_i for *i = 0,…, n -1*, E_{snake} is the energy function of snake, $E_{internal}$ is the internal elastic energy, E_{image} is forces that combine external energy of forces caused by the image, and E_{con} is the force caused by the image and the constraint force respectively.

Figure 3 shows the process of AC segmentation algorithm defining the mask initialization based on the parameter obtained from the fat and muscle in the object. Basically, the process is continued from image pre-processing labelled A.

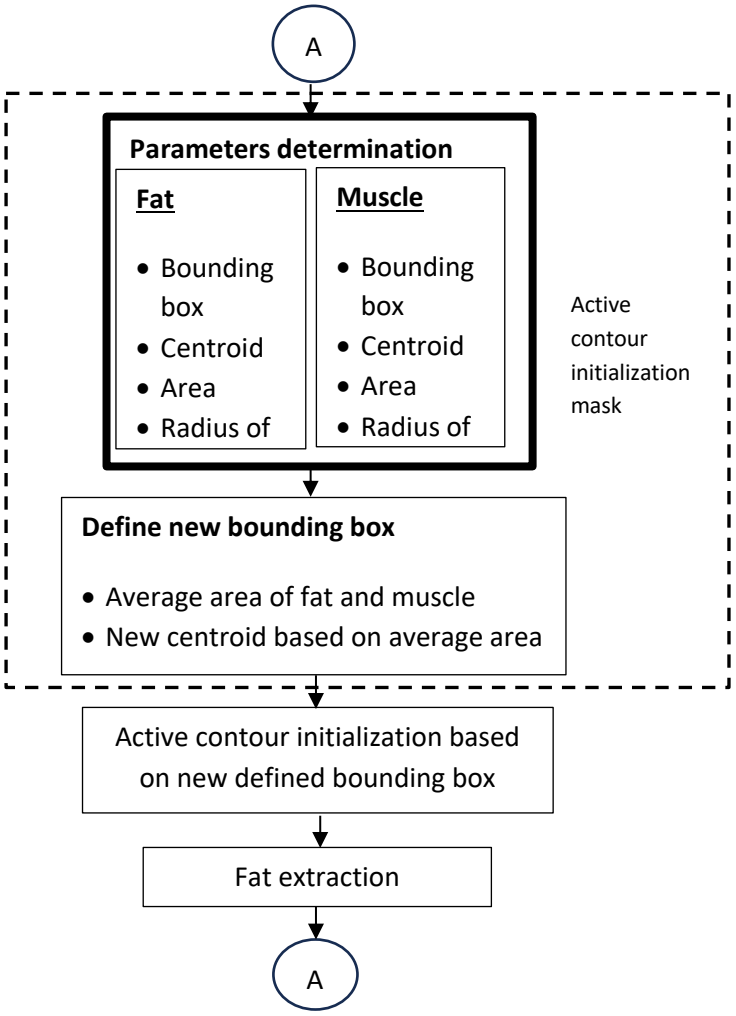

Fig. 3. The flowchart of AC mask initialization process

In the figure, the mask initialization is based on a few parameters on fat and muscle namely bounding box, centroid and radius of centroid. Next, the process is to define a new bounding box by determining the areas of both fat and muscle, which are then averaged to establish a new bounding box size. This updated bounding box dimension is subsequently employed to ascertain the appropriate dimensions for the ROI mask. Then, by averaging the centroids of fat and muscle, a new centroid is derived. This new centroid aids in identifying the minimum point of the bounding box, ensuring precise placement of the ROI mask. Hence, a new mask initialization box is defined.

The new defined bounding box is used as an initial curve for AC segmentation algorithm to extract the fat region in ROI. To optimize the segmentation, the size of the defined mask needs to be scaled down so that it will be placed between fat and muscle. The size of the average bounding box is

adjusted to specific values based on the characteristics of the image itself. Placing the bounding box directly on top of the thigh region simplifies the process of determining an appropriate value for achieving optimal segmentation. Next step is to select the number of iterations for AC algorithm. 500 iterations are selected, due to the shape, object of ROI and the size of MRI. In this study, 500 iterations can provide predictable movement pattern for the contour.

Figure 4(a) shows the original T1-Weighted image. The mask initialization is shown in Figure 4(b) where the white rectangular mask initialization box is placed onto the object between fat and muscle of the image. The mask initialization box is based on the area, bounding box and centroid of the fat and muscle.

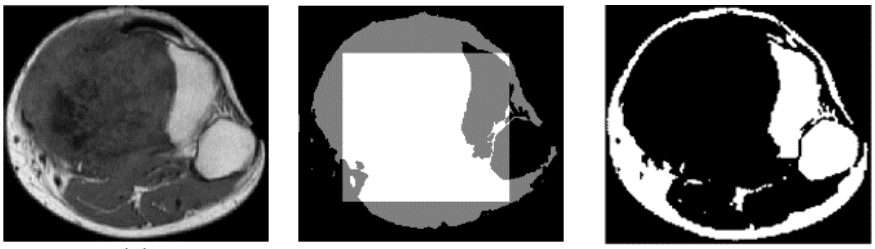

Fig. 4. (a) Original Image (b) Mask Initialization (c) Fat extraction

Finally, fat is extracted based on the initialization mask. It can be obvious that the initialization mask is placed between the fat and the muscle region. Figure 4(c) shows the fat is extracted from T1-Weighted when the initialization mask is defined correctly.

2.4 Performance Evaluation

To assess its overall performance, the values of True Positive (TP), True Negative (TN), False Positive (FP), and False Negative (FN) are determined:

i. True positive (TP) is when fat is correctly predicted as fat by AC algorithm based on ground truth image.
ii. True negative (TN) is when there is no fat and correctly predicted as no fat by AC algorithm based on ground truth image.
iii. False positive (FP) is described when there is no fat but incorrectly predicted as fat by AC algorithm based on ground truth image.
iv. False negative (FN) is when there is fat but incorrectly predicted as no fat.

The confusion matrix is formed based on the TP, TN, FP, and FN. The parameters in confusion matrix are determined by comparing the algorithm's segmentation results with the ground truth image. Figure 5 shows the confusion matrix that is used to describe the classifier performance in image processing. The confusion matrix summarizes the counts or percentages of pixels falling into each of these categories.

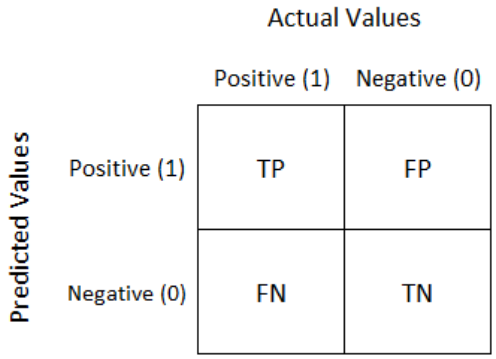

Fig. 5. Confusion matrix

The overall performance of the segmentation using the AC algorithm is evaluated by calculating metrics namely accuracy, precision, recall, and F1-Score, which can be derived from the obtained confusion matrix in Figure 5. Eq. (2), Eq. (3), Eq. (4) and Eq. (5) show the equation for the performance evaluation metrics.

$$Accuracy = \frac{TP+TN}{TP+FP+TN+FN} \tag{2}$$

$$Precision = \frac{TP}{TP+FP} \tag{3}$$

$$Recall = \frac{TP}{TP+FN} \tag{4}$$

$$F1\ score = \frac{2 \times Precision \times Recall}{Precision+Recall} \tag{5}$$

Accuracy, precision, recall and F1-score are important in determining the overall performance of the AC algorithm. Accuracy measures the overall correctness of a classification method by calculating the ratio of correctly predicted instances to the total number of instances. It provides a general assessment of how well the method performs across all classes. For precision, it quantifies the accuracy of the positive predictions. It is the ratio of true positive predictions to the total number of positive predictions made by the AC algorithm. Precision is useful in cases where false positives are costly or need to be minimized. Recall, also known as sensitivity or true positive rate, measures the ratio of true positive predictions to the total number of actual positive instances in the dataset. It quantifies the ability of the method to identify all positive instances correctly. Recall is important in scenarios where false negatives are costly or need to be minimized. Lastly, F1-score is a single metric that combines both precision and recall into a balanced measure of the method's performance. It is the harmonic means of precision and recall, providing a consolidated evaluation of the model's ability to balance between true positives and false negatives. F1-score gives equal importance to precision and recall, making it suitable for situations to find a balance between the two metrics.

3. Results and Discussion

In this study, all the experiments are run on a laptop with Intel Core i5-11400H 2.7Ghz processor and 16GB of RAM by using MATLAB software.

3.1 Image Pre-Processing

In the image pre-processing stage, the ROI is the foreground that needs to be extracted. To obtain an accurate AC segmentation, the unnecessary background pixel and objects that are connected to the border are removed. Multi-level thresholding method is applied to extract the fat. Figure 6(a) shows the original T1-Weighted image. Figure 6(b) shows the output of the binarize image after the pre-processing process. Due to inhomogeneity, the fat of the object cannot be covered fully. Morphological dilation is used to dilate and fill the object so that the object becomes one object to eliminate the inhomogeneity effect as shown in Figure 6(c). Figure 6(c) shows the resultant ROI mask after morphological and filling process.

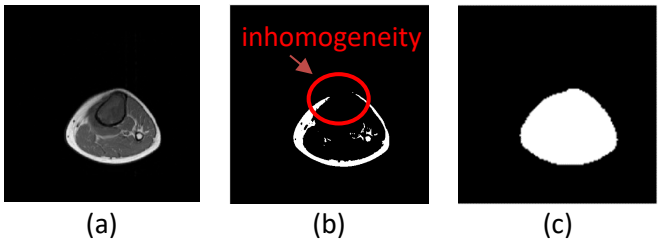

Fig. 6. (a) Original image (b) Binarize image (c) ROI mask

The bounding box of the ROI mask is defined and used to crop the ROI of the image. Figure 7 shows the output of the ROI. The background noise is then removed by assigning zero.

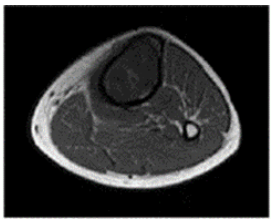

Fig. 7. ROI of the image

3.2 Automated Active Contour Segmentation

To execute the AC algorithm, the new defined initialization mask is placed onto the ROI. Due to the object shape and image size, 500 is set for the number of iterations for the AC segmentation. However, the average values obtained from the bounding boxes of the fat and muscle layers were not entirely precise. This is primarily because placing the mask on the entire muscle layer would result in over-segmentation. Figure 8(a) shows an example of oversized mask and Figure 8(b) shows an example of over-segmentation.

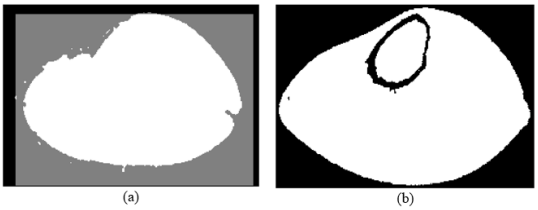

Fig. 8. (a) Oversized mask (b) Over-segmentation

To accurately place the mask, it is necessary to have a smaller bounding box for the muscle layer. However, determining the size of the bounding box can be subjective, as it depends on the size of the object and the quality of the MRI image produced by the machine. When the bounding box of the muscle layer is too small, the AC algorithm may not segment the object effectively, resulting in under-segmentation. Figure 9(a) shows an example of a small-sized mask and Figure 9(b) shows an example of under-segmentation.

Fig. 9. (a) Smaller mask (b) Under-segmentation

The accurate segmentation of the muscle and fat in the MRI thigh anatomical structure is achieved by using an appropriately sized mask. This eliminates the need for manual adjustment of the mask size to find the optimal placement. Figure 10(a) illustrates an example of precise mask placement and Figure 10(b) shows a successful segmentation of MRI thigh image. This mask size is the optimal placement for most of the images.

Fig. 10. (a) Accurate mask (b) Accurate segmentation

Figure 11 shows image outputs of the proposed mask initialization method for AC segmentation. Figure 11 shows that the mask initialization is succeeded by placing the mask onto the ROI. The initial mask is defined based on the average values of areas between fat and muscle. Based on the observation, the perfect mask initialization is when the mask is placed in between fat and muscle. The anatomy for image 1 and 2 in Figure 11 showed that the object had a thin fat layer. The mask is placed onto the ROI intercepting fat and muscle layers. Hence the segmentation process is done correctly by using Active Contour algorithm. The results of accuracy, precision, recall and F1-score for images 1 and 2 are shown in Table 1 with a score higher than 0.8.

Image 3 in Figure 11 showed that fat layers are thicker than images 1 and 2 had. The mask placement of image 3 is smaller due to the smaller size of muscle layers as shown in Figure 11. The accuracy, precision, recall and F1 score for image 3 are 0.955925, 0.910012, 0.979848 and 0.943640 respectively. Image 4 in Figure 11 shows that due the uneven magnetic distribution, the image is blur at the right top area. Image 5 in Figure 11 shows that the image is affected by inhomogeneity. In both cases, the mask initialization is difficult to define because the area of fat layers that intercepted with the mask was very small.

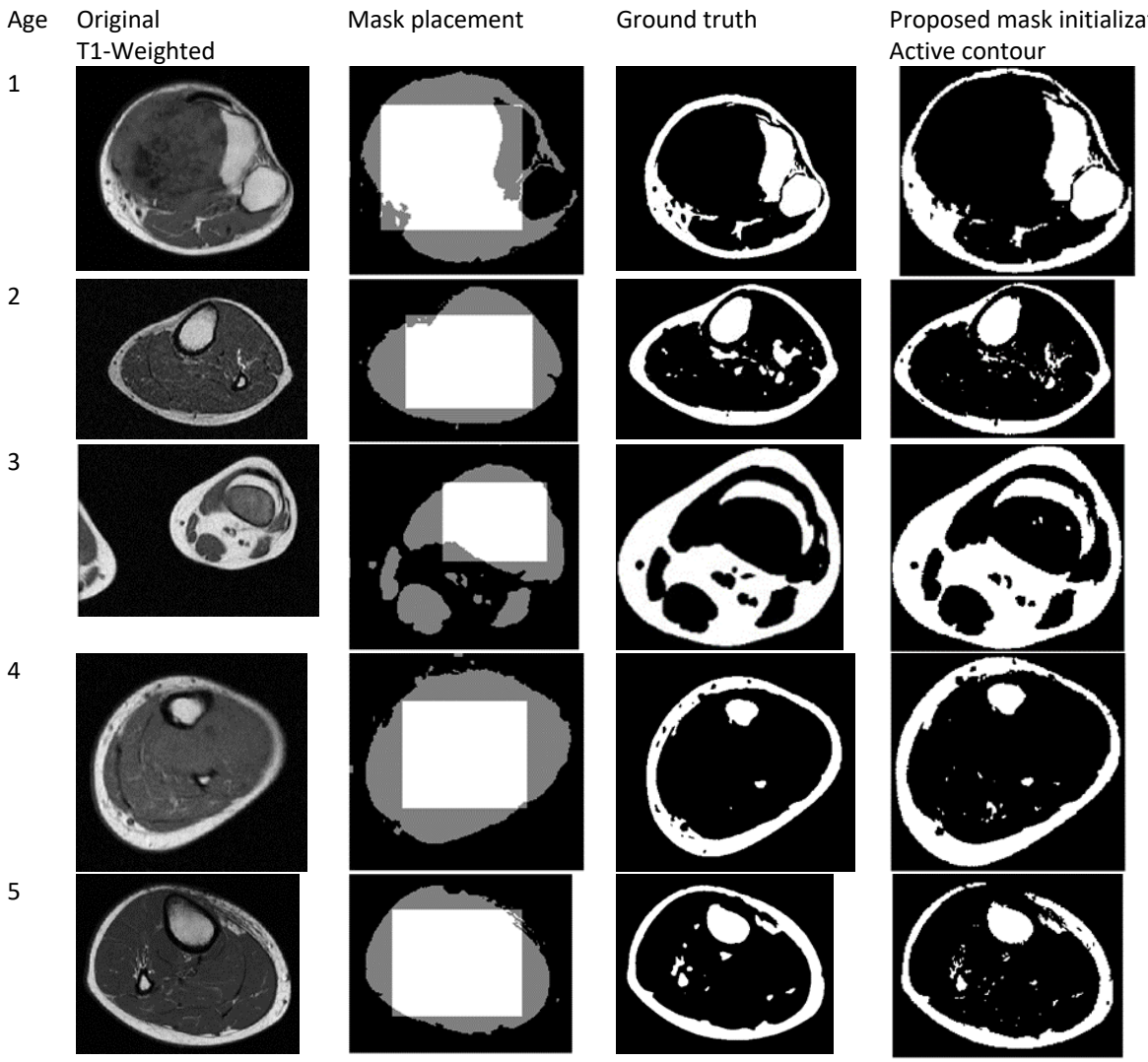

Fig. 11. The output of automated Active Contour (AC) segmentation

Table 1 shows the performance evaluation of the image outputs. However, the proposed mask initialization method for AC segmentation can define the initial mask for segmentation with results above 0.9 for accuracy, precision, recall and F1-score as shown in Table 1.

Table 1
Performance evaluation of images

Image	Accuracy	Precision	Recall	F1 Score
1	0.943104	0.980612	0.818364	0.892172
2	0.957607	0.994169	0.816730	0.896757
3	0.955925	0.910012	0.979848	0.943640
4	0.974600	0.919208	0.946621	0.932713
5	0.968007	0.988443	0.843121	0.910017

Table 2 shows the overall performance of 43 images. The values obtained for the accuracy, precision, recall and F1-score are all above 0.8. It signifies that the output produced using AC algorithm are similar with the ground truth image. It can be concluded that the mask initialization of

AC is performing well with the average values for accuracy, precision, recall and F1-score for all images are 0.92, 0.86, 0.88 and 0.89 respectively.

Table 2
Performance evaluation of 43 images

Image	Accuracy	Precision	Recall	F1-Score
C5S13	0.942397	0.981614	0.814991	0.890576
C5S14	0.965386	0.841647	0.945912	0.890738
C5S15	0.933381	0.731630	0.944809	0.824665
C5S16	0.956377	0.831682	0.885410	0.857705
C5S17	0.956956	0.993086	0.778099	0.872545
C5S18	0.934163	0.799649	0.853581	0.825735
C5S19	0.952242	0.935673	0.704523	0.803810
C5S20	0.892009	0.520946	0.884595	0.655728
C5S21	0.964936	0.690167	0.911920	0.785697
C5S22	0.957836	0.666543	0.856916	0.749835
C5S23	0.982591	0.949907	0.840186	0.891684
C5S24	0.956747	0.995001	0.812206	0.894359
C9S10	0.960303	0.978463	0.940824	0.959275
C9S11	0.929810	0.996577	0.866892	0.927222
C9S12	0.939061	0.899674	0.972140	0.934504
C9S13	0.953964	0.996069	0.898924	0.945007
C9S14	0.962341	0.978129	0.925983	0.951342
C9S15	0.915182	0.837801	0.954958	0.892551
C9S16	0.904695	0.794296	0.977799	0.876546
C9S17	0.970630	0.967499	0.942422	0.954796
C9S18	0.983375	0.955696	0.986751	0.970975
C9S19	0.957576	0.996117	0.874238	0.931207
C9S20	0.948878	0.977261	0.874847	0.923223
C9S21	0.964648	0.927429	0.974916	0.950580
C9S22	0.974493	0.985823	0.947629	0.966349
C9S23	0.951671	0.972403	0.910613	0.940494
C9S24	0.943737	0.880848	0.983644	0.929412
C14S10	0.812785	0.425731	0.979757	0.593549
C14S11	0.962267	0.923899	0.924609	0.924254
C14S12	0.889515	0.689745	0.950378	0.799353
C14S13	0.933444	0.822558	0.914451	0.866074
C14S14	0.900313	0.774067	0.921671	0.841445
C14S15	0.867381	0.706620	0.920432	0.799477
C14S16	0.955091	0.860447	0.935472	0.896393
C14S17	0.945557	0.907977	0.847933	0.876928
C14S18	0.939802	0.907627	0.829187	0.866636
C14S19	0.925821	0.992300	0.694995	0.817455
C14S20	0.945497	0.995529	0.737708	0.847442
C14S21	0.945386	0.995330	0.762664	0.863600
C14S22	0.963263	0.994997	0.812621	0.894609
C14S23	0.970253	0.994291	0.829062	0.904190
C14S24	0.966670	0.980799	0.804269	0.883805
C14S25	0.948083	0.825683	0.835220	0.830424
Average	0.92	0.86	0.88	0.89

4. Conclusions

A mask initialization method for AC algorithm is successfully defined. Based on the defined mask initialization, a segmentation system based on AC algorithm was developed. The system effectively

extracts fats in T1-Weighted images of long bone for OS patients. This study effectively extracted fat in MRI T1-Weighted sequence. By utilizing this algorithm, this study can be used to detect and isolate lesions associated with OS patients. Besides, it can be used to extract the abnormalities in other MRI sequences. Overall, this research contributes to the development of fat extraction systems for medical image analysis, specifically focusing on the long bone which is femur and tibia for MRI T1-Weighted sequence. The proposed mask initialization method for AC algorithm can be a great opportunity to extend to other bones for image analysis. The outcomes of this study have the potential to enhance clinical decision-making and improve the accuracy of diagnoses in the field of radiology.

Acknowledgement
Authors would like to thank Ministry of Education Malaysia for the Fundamental Research Funding grant (FRGS/1/2021/TK0/UITM/02/39), Universiti Teknologi MARA, Cawangan Pulau Pinang and Hospital USM for providing research facilities to run this study.

References

[1] Babacan, Serdar, and Mustafa Deniz. "Femur morphometry and correlation between proximal and distal parts." *Cukurova Medical Journal* 47, no. 1 (2022): 50-61. https://doi.org/10.17826/cumj.994863
[2] Czarnecka, Anna M., Kamil Synoradzki, Wiktoria Firlej, Ewa Bartnik, Pawel Sobczuk, Michal Fiedorowicz, Pawel Grieb, and Piotr Rutkowski. "Molecular biology of osteosarcoma." *Cancers* 12, no. 8 (2020): 2130. https://doi.org/10.3390/cancers12082130
[3] Khalifa, Hanadi M. "The awareness and attitude of medical radiologists toward oral and maxillofacial radiologists." *Medical Science* 24, no. 106 (2020): 4719-4725.
[4] Othman, Mohamad Haizan, Belinda Chong Chiew Meng, Nor Salwa Damanhuri, Mohd Ezane Aziz, and Nor Azlan Othman. "MRI Thigh Sequences in Determining the Tumor Size Using Fuzzy C-Means for Patients with Osteosarcoma." In *2022 IEEE 12th International Conference on Control System, Computing and Engineering (ICCSCE)*, pp. 125-130. IEEE, 2022. https://doi.org/10.1109/ICCSCE54767.2022.9935630
[5] Srinivasan, Kavitha, and N. M. Nanditha. "An intelligent skull stripping algorithm for MRI image sequences using mathematical morphology." *Biomed. Res* 29, no. 16 (2018): 3201-3206. https://doi.org/10.4066/biomedicalresearch.29-18-949
[6] Meng, Belinda Chong Chiew, Umi Kalthum Ngah, Bee Ee Khoo, Ibrahim Lutfi Shuaib, and Mohd Ezane Aziz. "A framework of MRI fat suppressed imaging fusion system for femur abnormality analysis." *Procedia computer science* 60 (2015): 808-817. https://doi.org/10.1016/j.procs.2015.08.243
[7] Malartre, Samuel, Damien Bachasson, Guillaume Mercy, Elissone Sarkis, Céline Anquetil, Olivier Benveniste, and Yves Allenbach. "MRI and muscle imaging for idiopathic inflammatory myopathies." *Brain Pathology* 31, no. 3 (2021): e12954. https://doi.org/10.1111/bpa.12954
[8] Gao, Jianqiang, Binbin Wang, Ziyi Wang, Yufeng Wang, and Fanzhi Kong. "A wavelet transform-based image segmentation method." *Optik* 208 (2020): 164123. https://doi.org/10.1016/j.ijleo.2019.164123
[9] Kon, Nasrul Azizi, Abdul Kadir Jumaat, and Muhammad Danial Adzlizan Suhaizi. "Active Contour Models for Boundary Extraction with Application to Medical Images with Noise." *Journal of Advanced Research in Applied Sciences and Engineering Technology* 33, no. 2 (2023): 300-312. https://doi.org/10.37934/araset.33.2.300312
[10] Hemalatha, R., T. Thamizhvani, A. Josephin Arockia Dhivya, Josline Elsa Joseph, Bincy Babu, and R. Chandrasekaran. "Active contour based segmentation techniques for medical image analysis." *Medical and Biological Image Analysis* 4, no. 17 (2018): 2. https://doi.org/10.5772/intechopen.74576
[11] Mohamed, Mohamed Ahmed Gilani, Wan Mahani Hafizah Wan Mahmud, and Raja Mohd Aizat Raja Izaham. "Hippocampus Segmentation of Brain MRI Images for Possible Progression Detection of Alzheimer's Disease." *Journal of Advanced Research in Applied Sciences and Engineering Technology* 32, no. 2 (2023): 234-241. https://doi.org/10.37934/araset.32.2.234241
[12] Keatmanee, Chadaporn, Utairat Chaumrattanakul, Kazunori Kotani, and Stanislav S. Makhanov. "Initialization of active contours for segmentation of breast cancer via fusion of ultrasound, Doppler, and elasticity images." *Ultrasonics* 94 (2019): 438-453. https://doi.org/10.1016/j.ultras.2017.12.008
[13] Radhi, Eman A., and Mohammed Y. Kamil. "Breast Tumor Detection Via Active Contour Technique." *International Journal of Intelligent Engineering & Systems* 14, no. 4 (2021). https://doi.org/10.22266/ijies2021.0831.49

[14] Mustafa, Saleem, Muhammad Waseem Iqbal, Toqir A. Rana, Arfan Jaffar, Muhammad Shiraz, Muhammad Arif, and Samia Allaoua Chelloug. "Entropy and Gaussian Filter-Based Adaptive Active Contour for Segmentation of Skin Lesions." *Computational Intelligence and Neuroscience* 2022 (2022). https://doi.org/10.1155/2022/4348235

[15] Huo, Jiawen, Aizhi Peng, Fenfang Chen, Fen Chen, Lanling Shen, and Hongxia Yan. "Efficacy Evaluation of Ultrasound with Active Contour Model for Hemodialysis in Children with Renal Failure." *Computational and Mathematical Methods in Medicine* 2022 (2022). https://doi.org/10.1155/2022/3665841

[16] Mewada, Hiren, Amit V. Patel, Jitendra Chaudhari, Keyur Mahant, and Alpesh Vala. "Composite fuzzy-wavelet-based active contour for medical image segmentation." *Engineering Computations* 37, no. 9 (2020): 3525-3541. https://doi.org/10.1108/EC-11-2019-0529

[17] Babu, KRajesh, NDurga Indira, K. Vara Prasad, and Syed Shameem. "An effective brain tumor detection from t1w MR images using active contour segmentation techniques." In *Journal of Physics: Conference Series*, vol. 1804, no. 1, p. 012174. IOP Publishing, 2021. https://doi.org/10.1088/1742-6596/1804/1/012174

[18] Ibrahim, Rabha W., Ali M. Hasan, and Hamid A. Jalab. "A new deformable model based on fractional Wright energy function for tumor segmentation of volumetric brain MRI scans." *Computer methods and programs in biomedicine* 163 (2018): 21-28. https://doi.org/10.1016/j.cmpb.2018.05.031

[19] Yusoff, Ainul Kamilah Mohd, Rafikha Aliana A. Raof, Norfadila Mahrom, Siti Suraya Md Noor, Fazrul Faiz Zakaria, and Phak Len. "Enhancement and Segmentation of Ziehl Neelson Sputum Slide Images using Contrast Enhancement and Otsu Threshold Technique." *Journal of Advanced Research in Applied Sciences and Engineering Technology* 30, no. 1 (2023): 282-289. https://doi.org/10.37934/araset.30.1.282289

[20] Kumar, Arpan, and Anamika Tiwari. "A comparative study of otsu thresholding and k-means algorithm of image segmentation." *Int. J. Eng. Technol. Res* 9 (2019): 2454-4698. https://doi.org/10.31873/IJETR.9.5.2019.62

[21] Houssein, Essam H., Bahaa El-din Helmy, Diego Oliva, Ahmed A. Elngar, and Hassan Shaban. "A novel black widow optimization algorithm for multilevel thresholding image segmentation." *Expert Systems with Applications* 167 (2021): 114159. https://doi.org/10.1016/j.eswa.2020.114159

[22] Su, Hang, Dong Zhao, Hela Elmannai, Ali Asghar Heidari, Sami Bourouis, Zongda Wu, Zhennao Cai, Wenyong Gui, and Mayun Chen. "Multilevel threshold image segmentation for COVID-19 chest radiography: A framework using horizontal and vertical multiverse optimization." *Computers in Biology and Medicine* 146 (2022): 105618. https://doi.org/10.1016/j.compbiomed.2022.105618

[23] Yang, Pei, Wei Song, Xiaobing Zhao, Rui Zheng, and Letu Qingge. "An improved Otsu threshold segmentation algorithm." *International Journal of Computational Science and Engineering* 22, no. 1 (2020): 146-153. https://doi.org/10.1504/IJCSE.2020.107266

[24] Al-Rahlawee, Anfal Thaer Hussein, and Javad Rahebi. "Multilevel thresholding of images with improved Otsu thresholding by black widow optimization algorithm." *Multimedia Tools and Applications* 80, no. 18 (2021): 28217-28243. https://doi.org/10.1007/s11042-021-10860-w